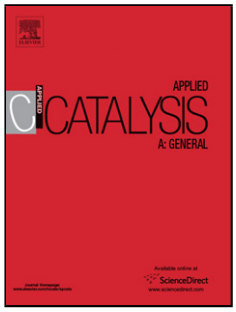

Title: The shape effect of $La_2O_2CO_3$ in Pd/$La_2O_2CO_3$ catalyst for selective hydrogenation of cinnamaldehyde

Authors: Fei Wang, Zhongnan Zhang, Xuejiao Wei, Qihua Fang, Xingmao Jiang

PII: S0926-860X(17)30296-X
DOI: http://dx.doi.org/doi:10.1016/j.apcata.2017.06.039
Reference: APCATA 16301

To appear in: *Applied Catalysis A: General*

Received date: 3-5-2017
Revised date: 29-6-2017
Accepted date: 30-6-2017

Please cite this article as: Fei Wang, Zhongnan Zhang, Xuejiao Wei, Qihua Fang, Xingmao Jiang, The shape effect of La2O2CO3 in Pd/La2O2CO3 catalyst for selective hydrogenation of cinnamaldehyde, Applied Catalysis A, Generalhttp://dx.doi.org/10.1016/j.apcata.2017.06.039

The Shape Effect of $La_2O_2CO_3$ in Pd/$La_2O_2CO_3$ Catalyst for Selective Hydrogenation of Cinnamaldehyde

Fei Wang[a,*], Zhongnan Zhang[a], Xuejiao Wei[b], Qihua Fang[a], Xingmao Jiang[a,c,*]

[a] *Advanced Catalysis and Green Manufacturing Collaborative Innovation Center, Changzhou University, Changzhou 213164, PR China.*

[b] *Department of chemical and Engineering, Changzhou Institute of Technology, Changzhou 213022, PR China.*

[c] *Key Laboratory for Green Chemical Process of Ministry of Education, Hubei Key Laboratory for Novel Reactor and Green Chemistry Technology, School of Chemical Engineering and Pharmacy, Wuhan Institute of Technology, Wuhan 430073, China*

** Corresponding author: E-mail: wangfei@cczu.edu.cn; jxm@cczu.edu.cn; jxm@wit.edu.cn Fax: +86-519-8633-0263; Tel: +86-519-8633-0253*

Graphical Abstract

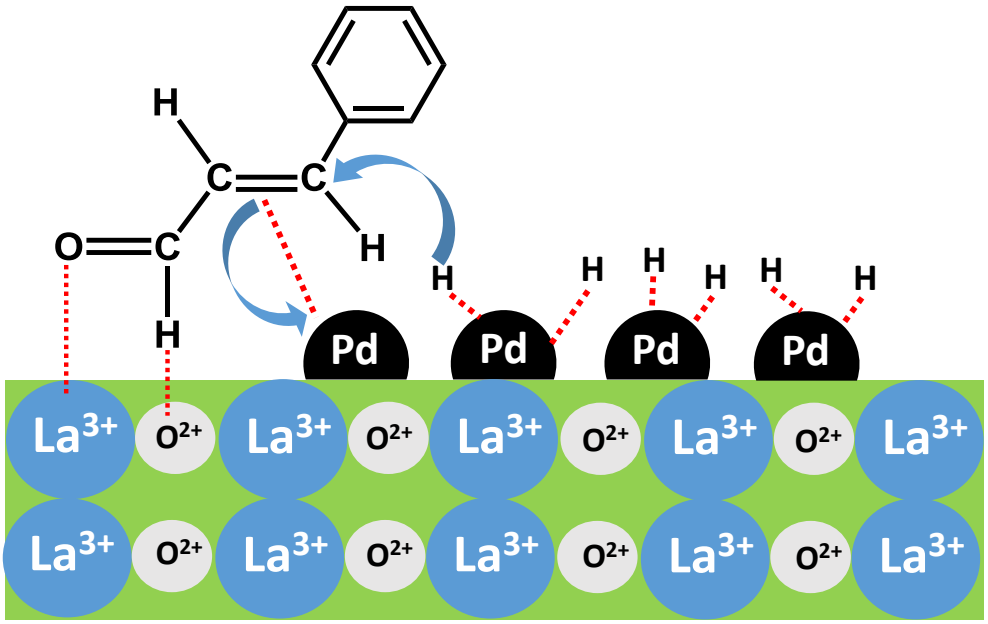

Highlights

- $Pd/La_2O_2CO_3$-NRs catalysts were successfully synthesized via hydrothermal method.
- $Pd/La_2O_2CO_3$-NRs catalyst exhibited better catalytic performance than $Pd/La_2O_2CO_3$-NPs catalyst for selective hydrogenation of CAL to HCAL.
- Support shape can modify surface basicity, which resulting in enhanced hydrogenation activity.
- $Pd/La_2O_2CO_3$-NRs catalyst is a highly efficient catalyst for selective hydrogenation of CAL to HCAL.

Abstract

Controllably adjusting the morphology of nanocatalysts is known as an effective way to improve catalytic performance. $Pd/La_2O_2CO_3$ catalysts with different morphologies (nanorods and nanoparticles) were successfully synthesized via simple hydrothermal method and evaluated for selective hydrogenation of cinnamaldehyde. The highly catalytic activity (86 % HCAL selectivity at 100 % CAL conversion at 3 h) occurred over $Pd/La_2O_2CO_3$-NRs with $La_2O_2CO_3$ nanorods as support. Remarkably, $Pd/La_2O_2CO_3$-NRs catalyst not only showed better catalytic performance, nearly 10 times higher than $Pd/La_2O_2CO_3$-NPs catalyst, but also exhibited excellent cycling stability. CO_2-TPD showed that the intense desorption peaks at about 560 K represented the medium-strength basic sites (La^{3+}-O^{2-} pairs) with a total amount of 0.13 mmol g^{-1} on the $La_2O_2CO_3$-NPs and 0.21 mmol g^{-1} on the $La_2O_2CO_3$-NRs. These results indicated that support morphology has a significant effect on catalytic activity and can modify surface basicity, which resulting in enhanced hydrogenation activity.

Keywords: Palladium; $La_2O_2CO_3$ nanorods; Cinnamaldehyde hydrogenation; Shape effect; Basicity

1. Introduction

Selective hydrogenation of α, β-unsaturated aldehydes to the corresponding unsaturated alcohols is highly attractive because it is an essential step in the synthesis of value-added fine chemicals [1]. For example, selective hydrogenation of cinnamaldehyde (CAL) route was shown in Scheme 1,

which can produce cinnamal alcohol (COL), hydrocinnamaldehyde (HCAL), hydrocinnamal alcohol (HCOL) [2]. Formed HCAL through hydrogenation of the C=C bond were found as an essential organic intermediate for the preparation of drugs in the treatment of HIV [3].

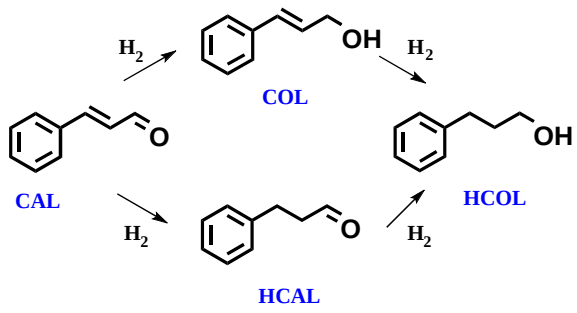

Scheme 1 Reaction pathways for selective hydrogenation of CAL

Many metals such as Ni [4], Cu [5], Os [6], Ir [7], Pt [8], Ru [9], Au [10], Pd [11] and so on, have been proved as highly efficient catalysts for the activation of C=C and C=O bonds. Among them, the Pd-based catalysts are considered to be one of the most promising active center for selective oxidation [12], Suzuki coupling reaction [13] and especially the selective hydrogenation of the C=C bond [14]. Recently, Liao et al. [15] reported a high-performance bimetallic PdAu catalyst with mesoporous silica nanoparticles as prepared by an organic impregnation-hydrogen reduction approach, which showed up to four times higher activity than that of Pd/MSN (without Au as a promoter) and eight times higher activity than that of commercial Pd/C catalyst. Liu et al. [16] also found that smaller Pd particles preferred a higher selectivity to C=C bond hydrogenation, forming HCAL, while on larger ones, the selectivity to C=O bond hydrogenation increased yielding a higher selectivity to COL. Except adding other metal as promoter and controlling the size of metal particles, support effect seems to be an important factor adjusting the catalytic activity and selectivity to C=C bond [17]. Metal oxide nanomaterials as the catalyst supports were reported to be able to improve the activity and selectivity to COL [18]. Previous reports [19] demonstrate that the shape of the metal oxide particle at the nanometre scale is essentially important for obtaining highly active and selective performance through selective exposure of the reactive facets and that morphological control could greatly promote the catalytic performance by enriching the surface active sites. Up to date, there are very few reports about the shape effect of support on the catalytic performance of hydrogenation of CAL. Previously, we have reported [20] that copper nanoparticles dispersed rod-

shaped $La_2O_2CO_3$ efficiently catalyzed transfer dehydrogenation of primary aliphatic alcohols with an aldehyde yield of up to 97 %. These results show that the (110) planes of the $La_2O_2CO_3$ support not only provided a substantial number of medium-strength basic sites for activating the alcohol but also directed the selective dispersion of copper particles approximately 4.5 nm in size on their surfaces.

In this study, we extended the application of the $La_2O_2CO_3$ nanorods support to selective hydrogenation of CAL. Herein, we reported an active and stable catalyst, Pd nanoparticles dispersed on $La_2O_2CO_3$ nanorods. The resulting catalyst displayed obviously enhanced catalytic activity for hydrogenation of CAL to HCAL. Compared with Pd nanoparticles dispersed on $La_2O_2CO_3$ nanoparticles catalyst, this enhancement can be rationalized by basicity of $La_2O_2CO_3$.

2. Experimental section

2.1 Materials synthesis

The $La(OH)_3$ nanorods were prepared by a hydrothermal method from our previous work [20]. 1.0 g of $La(NO_3)_3{\cdot}6H_2O$ was dissolved in 20 mL of water, and the mixture was added to 60 mL of aqueous 5.0 M KOH solution, yielding a white precipitate. The slurry was transferred into an autoclave (100 mL), heated to 453 K and maintained at that temperature for 12 h. The solid product was washed with water and dried at 323K under vacuum, giving $La(OH)_3$ nanorods. Calcination of this lanthanum hydroxide precursor at 773K for 4 h in air produced $La_2O_2CO_3$ nanorods. $La(OH)_3$ nanoparticles were prepared by simple precipitation method and other conditions were same as $La(OH)_3$ nanorods.

The $Pd/La_2O_2CO_3$ catalyst was prepared by a deposition-precipitation method. A certain amount $Pd(NO_3)_3$ was dissolved in 120 ml of water, and 0.5 g of $La_2O_2CO_3$ nanorods (or nanopaticles) was dispersed into the solution at room temperature. Aqueous 0.1 M NaOH solution was added dropwise to the mixture. Addition of NaOH used to adjust the pH=8-9 and then the precipitate was aged for 2 h at room temperature. The resulting solid was washed with water, dried at 383 K overnight and calcined at 723 K for 4 h in air, forming $PdO/La_2O_2CO_3$. 200 mg of this catalyst precursor was treated with pure hydrogen (40 ml min^{-1}) at 573 K for 1 h in a fixed-bed reactor, yielding the $Pd/La_2O_2CO_3$ catalyst.

2.2 Structure analyses

X-ray powder diffraction (XRD) patterns were recorded on a D/MAX 2500/PC powder diffractometer (Rigaku) using a CuKα radiation source operated at 40 kV and 200 mA from 5 ° to 70 ° (in 2 θ) with the scanning rate of 20 ° min^{-1}. X-ray photoelectron spectroscopy (XPS) was operated using Thermo Scientific Escalab 250 instrument under ultrahigh vacuum with a pressure close to 2×10^{-9} mbar. Transmission electron microscope (TEM, JEOL JEM-2100) was applied for the detailed microstructure and composition information. The surface area was measured by the surface area and pore size analyzer (Autosorb-iQ2-MP). The palladium content in the prepared catalysts was determined by an inductively coupled plasma atomic emission spectrometry (ICP-AES).

Temperature programmed desorption of CO_2 on the samples was carried out with a U-shape quartz tubular reactor. The sample (100 mg) was exposed to a mixture of 30 vol.% CO_2/He (30 ml min^{-1}) for 0.5 h at 423 K. After being purged with He (30 ml min^{-1}) for 2 h, the sample was heated to 1073 K at a rate of 5 K min^{-1}; the amount of CO_2 desorbed was monitored by an on-line mass spectrometer.

2.3 Catalytic test

Selective hydrogenation of CAL was conducted in a stainless steel autoclave (50 ml). Typically, the reaction mixture contained 1.0 mL CAL, 20 mL ethanol (solvent) and 100 mg $Pd/La_2O_2CO_3$ catalyst. During the hydrogenation, catalysts were suspended in solution by violent stirring. The reaction was performed at 333-363 K for a certain period (0.5–3 h) under 1.0 MPa H_2 pressure. At the end of the reaction, the reactor was cooled to the ambient temperature, and the catalysts were separated from the reaction mixture. The catalysts were recycled and reused in the next reaction. The product of each hydrogenation reaction was analyzed by Haixin GC-950 gas chromatography (HP-5 capillary column).

3. Results and discussion

3.1. Structural characteristics of the catalysts

The phase purity of the products was examined by X-ray diffraction (XRD) measurement performed on Rigaku X-ray diffractometer with Cu Kα radiation. As shown as Fig. 1, the peaks at about 23 °,

29 °, and 44° for $La_2O_2CO_3$-NPs sample can be indexed to (110), (130), and (200) phases, corresponding to a monoclinic structure for $La_2O_2CO_3$ (JCPDS No. 48-1113), while the peaks at about 26 °, 27 °, 31 °, and 45° for $La_2O_2CO_3$-NRs sample can be indexed to (100), (101), (103), and (110) phases, corresponding to hexagonal phase of $La_2O_3CO_3$ (JCPDS card 37-0804) [21]. After loading Pd, an almost identical XRD pattern was obtained for Pd/$La_2O_2CO_3$-NPs comparing with $La_2O_2CO_3$-NPs. Moreover, Pd/$La_2O_2CO_3$-NRs also showed same structure as $La_2O_2CO_3$-NRs, indicating the crystalline structure and the average size of the crystalline domain of the support were well maintained in the Pd samples. No peaks due to metallic Pd were detected, owing to the fact that the Pd particle sizes were very small (<5 nm).

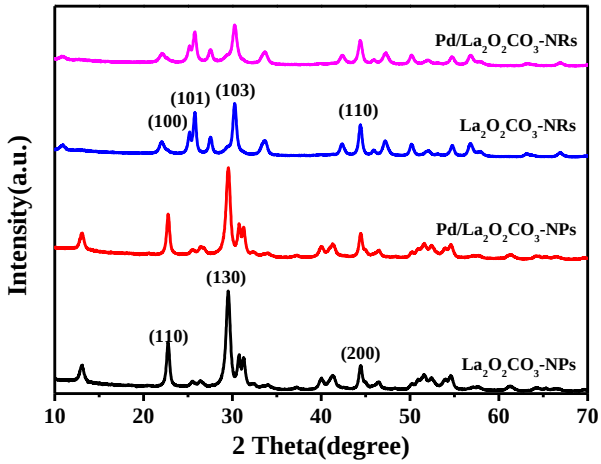

Fig. 1 XRD patterns of $La_2O_2CO_3$-NPs, $La_2O_2CO_3$-NRs, Pd/$La_2O_2CO_3$-NRs and Pd/$La_2O_2CO_3$-NPs samples.

The shapes of the obtained samples were analyzed by TEM (Fig. 2). The as-obtained $La_2O_2CO_3$-NRs were 200–300 nm in length and about 15-20 nm in diameter (Fig. 2a). In their HRTEM images (Fig. 2b), the Pd nanoparticles were dispersed effectively on the surface of the $La_2O_2CO_3$-NRs synthesized at 180 °C for 12 h and are not agglomerated. And supported Pd particles in Pd/$La_2O_2CO_3$-NRs catalysts exhibit similar polyhedral shapes, and the Pd nanoparticles on the $La_2O_2CO_3$-NRs have crystallite sizes between 3.0 and 3.5 nm. This result was in accordance with XRD results. On the other hand, the $La_2O_2CO_3$-NPs exhibited irregular shapes and their agglomeration can be observed (Fig. 2c). Fig. 2d showed that the Pd particle size distribution reflect the uniform distribution with an average particle size of 3.0–3.5 nm as same as Pd/$La_2O_2CO_3$-NRs

catalysts.

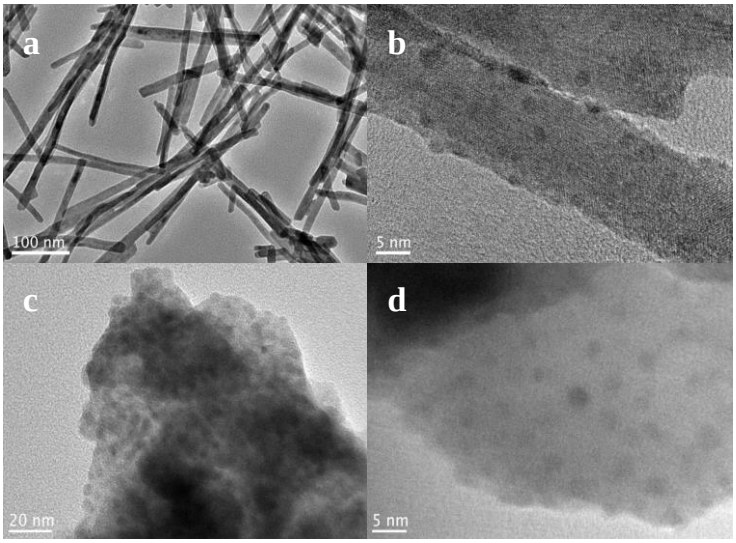

Fig. 2 TEM and HRTEM images of $La_2O_2CO_3$-NRs (a), Pd/$La_2O_2CO_3$-NRs (b) and Pd/$La_2O_2CO_3$-NPs (c, d) samples

Table 1 summarizes the physical and chemical properties of the Pd/$La_2O_2CO_3$-NRs and Pd/$La_2O_2CO_3$-NPs samples. Surface area of Pd/$La_2O_2CO_3$-NRs sample was 54.2 m^2 g^{-1}, while surface area of Pd/$La_2O_2CO_3$-NPs was only 20.6 m^2 g^{-1}. To investigate the base characteristics of catalysts, which are crucial to the selective hydrogenation of CAL, the CO_2 adsorption of Pd/$La_2O_2CO_3$-NPs and Pd/$La_2O_2CO_3$-NRs materials with different support morphologies were studied (Fig. 3). Desorption peaks located at 323-423 K, 423-673 K, 673-1073 K are attributed to the weak, medium-strength and strong basic sites, respectively [22]. The amount of CO_2 desorbed from these base sites were calculated and displayed in Table 1. It can be noted that surface of Pd/$La_2O_2CO_3$-NRs exposed more amount of weak and medium-strength basic sites (totally 0.21 mmol g^{-1}) than Pd/$La_2O_2CO_3$-NPs (0.13 mmol g^{-1}). These results indicated that support morphology can modify surface basicity.

Table 1 Physical and chemical properties of Pd/$La_2O_2CO_3$-NPs and Pd/$La_2O_2CO_3$-NRs samples.

Sample	Pd content[a] (wt%)	S_{BET}[b] (m^2 g^{-1})	Amount of basicity[c] (mmol g^{-1})		
			Weak basic sites	Medium-strength basic sites	Total
Pd/$La_2O_2CO_3$-NPs	0.99	20.6	0.02	0.11	0.13
Pd/$La_2O_2CO_3$-NRs	0.98	54.2	0.05	0.16	0.21

[a] Determined by ICP-AES. [b] BET surface area. [c] Estimated from the CO_2–TPD profiles in Fig. 3.

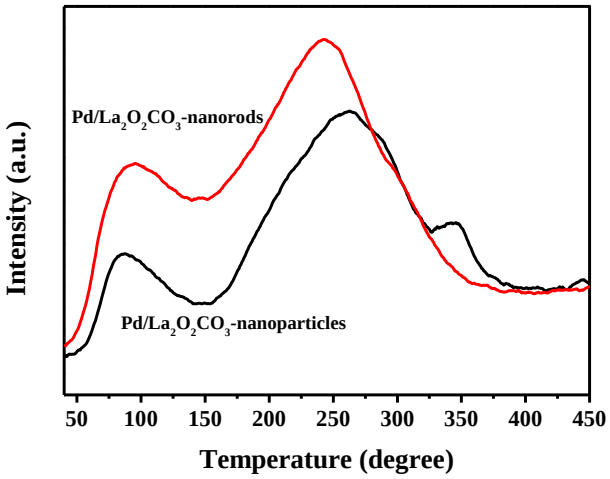

Fig. 3 CO_2-TPD profiles of Pd/$La_2O_2CO_3$-NRs and Pd/$La_2O_2CO_3$-NPs samples.

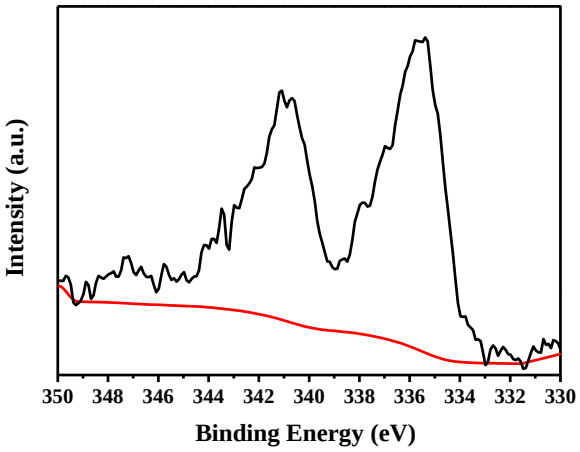

Fig. 4 Pd 3d XPS spectra of of Pd/$La_2O_2CO_3$-NRs sample.

XPS was used to check the oxidation state of the reduced and heat-treated Pd/$La_2O_2CO_3$-NRs catalysts. As shown as Fig. 4, the Pd spectrum showed two weak peaks associated with Pd $3d_{3/2}$ and Pd $3d_{5/2}$ at around 340.9 and 335.1 eV, respectively. These values clearly indicate the existence of Pd in metallic form on the surface of $La_2O_2CO_3$-NRs support (B.E. value of Pd $3d_{5/2}$ in metallic form is 335.2 eV) [23]. Weak peaks and some burrs probably owes to small size and high-dispersity of Pd nanoparticles.

3.2 Catalytic activity in hydrogenation of CAL

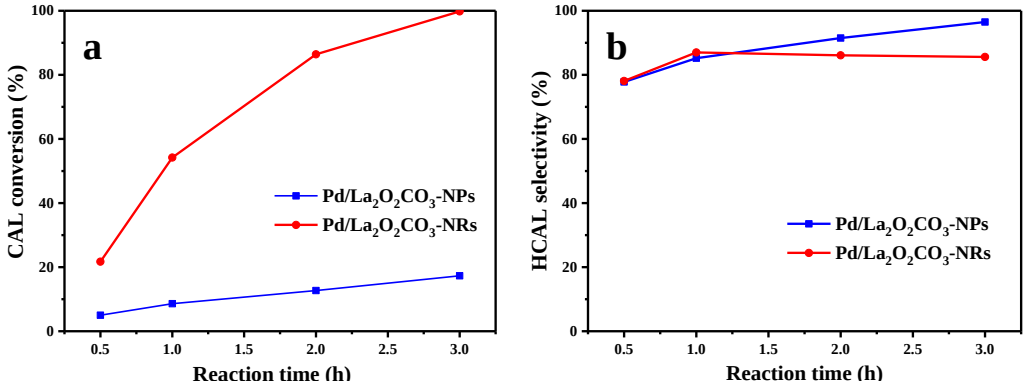

Fig. 5 (a) CAL conversion and (b) HCAL selectivity as a function of reaction time over $Pd/La_2O_2CO_3$-NPs (blue curve) and $Pd/La_2O_2CO_3$-NRs (red curve) samples. Reaction conditions: CAL (1 mL); catalyst (100 mg); solvent (ethanol, 20 mL); H_2 pressure (0.1 MPa); temperature (80 °C); stirring speed (800 rpm).

Catalytic tests in selective hydrogenation of CAL were performed over $Pd/La_2O_2CO_3$ catalysts with the different morphologies support of nanorods, nanoparticles and the results were presented in Fig. 5. The catalytic activity of the two $Pd/La_2O_2CO_3$ catalysts increased with extending the reaction time. However, The CAL conversion over the $Pd/La_2O_2CO_3$-NRs sample using nanorods as support was close to 100 % for 3 h, whereas the $Pd/La_2O_2CO_3$-NPs using nanoparticles as support sample showed only around 18 % CAL conversion for 3 h. We also compared the TOFs of HCAL produced by these two catalysts. Remarkably, $Pd/La_2O_2CO_3$-NRs catalyst showed better catalytic performance (0.3 s^{-1}), nearly 10 times higher than $Pd/La_2O_2CO_3$-NPs catalyst (0.04 s^{-1}). As shown as Table 2, the obtained activities for the $Pd/La_2O_2CO_3$-NRs catalysts were compared with previous reports to demarcate superiority of the present catalysts systems [24-28]. D. Srinivas et al. [29] reported that alkali ions facilitate adsorption of CAL through polarization of the carbonyl of CAL. This enhanced adsorption of CAL molecules and electronic effects are the causes for more efficient activity of $Pd/La_2O_2CO_3$ catalysts in presence of alkali solution. Combining CO_2-TPD results, the more medium-strength basic sites on $Pd/La_2O_2CO_3$-NRs sample using nanorods as support is, the more adsorption of CAL is on its surface, which resulting in enhanced reaction activity. It can be clearly seen that more medium-strength basic sites were favorable for the catalytic performance. Although more CAL was absorbed on $La_2O_2CO_3$-NRs support by C=O bond, the hydrogenation activity of Pd for C=O bond was much weaker than for C=C bond [30]. Thus, the main product was

still HCAL by the hydrogenation C=C of CAL over Pd/$La_2O_2CO_3$ catalyst. These results suggested that increase of basic sites could promote hydrogenation rate, but product selectivity was not affected in presence of Pd. The enhanced catalytic activity may result from the morphology effect of $La_2O_2CO_3$ supports.

Table 2 Comparison of the activity reported of catalysts for the CAL hydrogenation.

Catalysts	Pd content (wt%)	Reaction time (h)	CAL conversion (%)	HCAL selectivity (%)	Ref.
Pd/$La_2O_2CO_3$-NRs	0.98	3	100	86	This work
Pd/$La_2O_2CO_3$-NPs	0.99	3	17	96	This work
Pd/MWNTs	5.0	25	100	81	24
Pd/CeO_2-ZrO_2	2.0	8	79	90	25
Pd/ZIF-8	1.0	6	100	91	26
Pd@TNTs	2.5	7	100	82	27
Pd/NMC	2.05	4	100	93	28

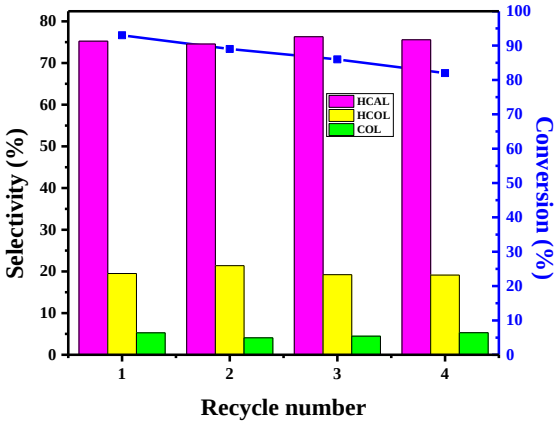

Fig. 6 Recyclability study of Pd/$La_2O_2CO_3$-NRs catalyst in the CAL hydrogenation. Reaction conditions: CAL (1 mL); catalyst (100 mg); solvent (ethanol, 20 mL); H_2 pressure (0.1 MPa); temperature (80 °C); stirring speed (800 rpm).

The recyclability of Pd/$La_2O_2CO_3$-NRs catalyst was investigated through a four-run recycling test in selective hydrogenation of CAL. As shown as Fig. 6, recycling tests verified that the conversion of CAL decreases slightly from 93 % to 82 % while the selectivity of HCAL keeps constant at a very high level of 75 %, which indicating that Pd/$La_2O_2CO_3$-NRs catalyst exhibited excellent cycling stability. Based on XRD and TEM results (Fig. 7), the loss of catalytic activity may be

mainly due to the minor rupture of $La_2O_2CO_3$ nanorods and aggregation of Pd nanoparticles.

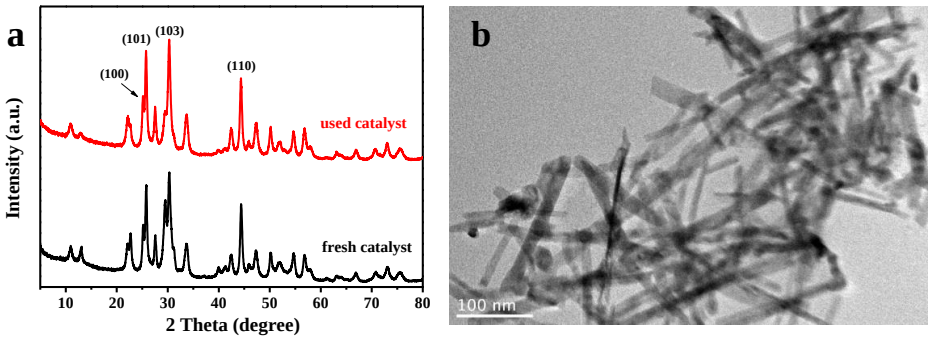

Fig. 7 (a) XRD patterns of fresh and used Pd/$La_2O_2CO_3$-NRs catalyst in the CAL hydrogenation. (b) TEM image of used Pd/$La_2O_2CO_3$-NRs catalyst in the CAL hydrogenation.

Based on the literature and our results, a brief reaction mechanism of CAL hydrogenation over Pd/$La_2O_2CO_3$-NRs catalyst was proposed, which is shown in Fig. 8. Firstly, the C=O group in CAL was preferentially adsorbed and activated by La^{3+}-O^{2-} pairs (medium-strength basic sites) at $La_2O_2CO_3$ support. Meanwhile, hydrogen was dissociated on the surface of Pd nanoparticles. While because the chemisorption of C=C bond over the Pd metal catalysts becomes more favorable than C=O bond, the selective hydrogenation of C=C bond preferably occurs by the attack of the activated hydrogen species and the resulting atomic hydrogen reacted with the activated C=C group, forming HCAL. Hence, surface basicity accelerated activation of C=C bond and promote the reaction.

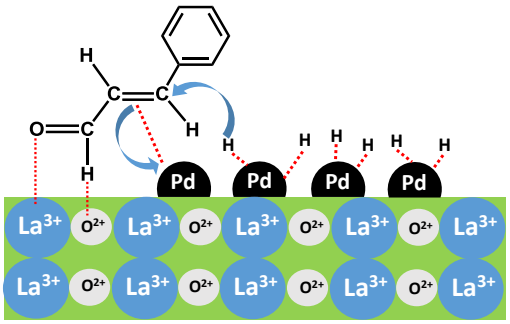

Fig. 8 Possible reaction mechanism of CAL hydrogenation on Pd/$La_2O_2CO_3$-NRs catalyst.

4. Conclusion

In summary, we successfully synthesis $La_2O_2CO_3$ nanomaterials with different morphologies (nanorods and nanoparticles) and then Pd nanoparticles were uniformly dispersed on them by

deposition-precipitation method. The catalytic activities of Pd/$La_2O_2CO_3$ catalysts for selective hydrogenation of CAL were investigated. It has been observed that the Pd/$La_2O_2CO_3$-NRs catalyst exhibits higher hydrogenation rate (0.3 s^{-1}) and excellent cycling stability, whereas Pd dispersed on $La_2O_2CO_3$ nanoparticles (Pd/$La_2O_2CO_3$-NPs) showed relatively low catalytic activities (0.04 s^{-1}). This difference in catalytic activities was attributed to basicity of $La_2O_2CO_3$ supports. CO_2-TPD showed that the intense desorption peaks at about 560 K represented the medium-strength basic sites (La^{3+}-O^{2-} pairs) with a total amount of 0.13 mmol·g^{-1} on the $La_2O_2CO_3$-NPs and 0.21 mmol·g^{-1} on the $La_2O_2CO_3$-NRs. These results suggested that increase of basic sites could obviously promote hydrogenation rate, but product selectivity was not affected in presence of Pd. The enhanced catalytic activity may result from the morphology effect of $La_2O_2CO_3$ supports. Consequently, the Pd/$La_2O_2CO_3$-NRs catalyst is a highly efficient catalyst for selective hydrogenation of CAL to HCAL.

Acknowledgments

This work was financially supported by the National Natural Science Foundation of China (No. 21503023) and Advanced Catalysis and Green Manufacturing Collaborative Innovation Center, Changzhou University.

References

[1] C. M. Piquerasa, V. Pucciaa, D. A. Vegab, M. A. Volpe, Appl. Catal. B 185 (2016) 265–271.

[2] Y. J. Zhu and F. Zaera, Catal. Sci. Technol. 4 (2014) 955–962.

[3] P. Mäki-Arvela, J. Hájek, T. Salmi, D. Y Murzin, Appl. Catal. A 292 (2005) 1–49.

[4] M. G. Prakash, R. Mahalakshmy, K. R. Krishnamurthy and B. Viswanathan, Catal. Sci. Technol. 5 (2015) 3313–3321.

[5] S. Rana and S. B. Jonnalagadda, RSC Adv. 7 (2017) 2869–2879.

[6] R. A. Sánchez-Delgado, M. Medina, F. López-Linares, A. Fuentes, J. Mol. Catal. A 116 (1997) 167–177.

[7] J. P Breen, R. Burch, J. Gomez-Lopez, K. Griffin, M. Hayes, Appl. Catal. A 268 (2004) 267–

274.

[8] S. P. Wei, Y. T. Zhao, G. L. Fan, L. Yang, F. Li, Chem. Eng. J. 322 (2017) 234–245.

[9] H. J. Shen, H. D. Tang, H. Y. Yan, W. F. Han, Y. Li and J. Ni, RSC Adv. 4 (2014) 30180–30185.

[10] C. H. Hao, X. N. Guo, Y. T. Pan, S. Chen, Z. F. Jiao, H. Yang, and X. Y. Guo, J. Am. Chem. Soc. 138 (2016) 9361–9364.

[11] S. J. Chen, L. Meng, B. X. Chen, W. Y. Chen, X. Z. Duan, X. Huang, B. S. Zhang, H. B. Fu, and Y. Wan, ACS Catal. 7 (2017) 2074–2087.

[12] S. Rana, S. Maddila and S. B. Jonnalagadda, Catal. Sci. Technol. 5 (2015) 3235–3241.

[13] S. Rana, S. Maddila, K. Yalagala, S. B. Jonnalagadda, Appl. Catal. A 505 (2015) 539–547.

[14] Y. K Zhang, S. J Liao, Y. Xu, D. R. Yu, Appl. Catal. A 192 (2000) 247–251.

[15] X. Yang, D. Chen, S. J. Liao, H. Y. Song, Y. W. Li, Z. Y. Fu, Y. L. Su, J. Catal. 291 (2012) 36–43.

[16] F. Jiang, J. Cai, B. Liu, Y. B. Xu and X. H. Liu, RSC Adv. 6 (2016) 75541–75551.

[17] Y. F. Zhang, S. H. Zhang, X. L. Pan, M. Bao, J. H. Huang, W. J. Shen, Catal. Lett. 147 (2017) 102–109.

[18] M. M. Wang, L. He, Y. M. Liu, Y. Cao, H. Y. He and K. N. Fan, Green Chem. 13 (2011) 602–607.

[19] Y. Li, W. J. Shen, Chem. Soc. Rev. 43 (2014) 1543–1574.

[20] F. Wang, R.J. Shi, Z. Q. Liu, P. J. Shang, X. Y. Pang, S. Shen, Z. C. Feng, C. Li, and W. J. Shen, ACS Catal. 3 (2013) 890–894.

[21] Q. Y. Mu, Y. D. Wang, J. Alloys Compd. 509 (2011) 396–401.

[22] F. Wang, N. Ta, Y. Li, W. J. Shen, Chin. J. Catal. 35 (2014) 437–443.

[23] J. C. Hierso, C. Satto, R. Feurer and P. Kalck, Chem. Mater. 8 (1996) 2481–2485.

[24] J. Philippe, L. Pesant, G. Ehret, M. J. Ledoux, C. P. Huu, Appl. Catal. A 288 (2005) 203–210.

[25] S. Bhogeswararao, D. Srinivas, Catal. Lett. 140 (2010) 55–64.

[26] Y. Zhao, M. M. Liu, B. B. Fan, Y. F. Chen, W. M. Lv, N. Y. Lu, R. F. Li, Catal. Comm. 57 (2014) 119–123.

[27] X. Yang, L. P. Wu, L. L. Ma, X. J. Li, T. J. Wang, S. J. Liao, Catal. Comm. 59 (2015) 184–188.

[28] A. S. Nagpure, L. Gurrala, P. Gogoi and S. V. Chilukuri, RSC Adv. 6 (2016) 44333–44340.

[29] S. Bhogeswararao, V. Pavan Kumar, K. V. R. Chary, D. Srinivas, Catal. Lett. 143 (2013) 1266–1276.

[30] A. M. R. Galletti, C. Antonetti, A. M. Venezia, G. Giambastiani, Appl. Catal. A 386 (2010) 124−131.